Journal of Magnetic Resonance 226 (2013) 45–51

Contents lists available at SciVerse ScienceDirect

Journal of Magnetic Resonance

journal homepage: www.elsevier.com/locate/jmr

Longitudinal NMR parameter measurements of Japanese pear fruit during the growing process using a mobile magnetic resonance imaging system

Yuto Geya [a], Takeshi Kimura [a], Hirotaka Fujisaki [a], Yasuhiko Terada [a], Katsumi Kose [a,*], Tomoyuki Haishi [b], Hiroshi Gemma [c], Yoshihiko Sekozawa [c]

[a] Institute of Applied Physics, University of Tsukuba, 1-1-1 Tennodai, Tsukuba 3058573, Japan
[b] MRTechnology Inc., 2-1-6 B5 Sengen, Tsukuba 3050047, Japan
[c] Agricultural and Forestry Research Center, University of Tsukuba, 1-1-1 Tennodai, Tsukuba 3058577, Japan

ARTICLE INFO

Article history:
Received 2 May 2012
Revised 18 October 2012
Available online 15 November 2012

Keywords:
MRI
Relaxation time
ADC
Fruit

ABSTRACT

Longitudinal nuclear magnetic resonance (NMR) parameter measurements of Japanese pear fruit (*Pyrus pyrifolia* Nakai, Kosui) were performed using an electrically mobile magnetic resonance imaging (MRI) system with a 0.2 T and 16 cm gap permanent magnet. To measure the relaxation times and apparent diffusion coefficients of the pear fruit in relation to their weight, seven pear fruits were harvested almost every week during the cell enlargement period and measured in a research orchard. To evaluate the *in situ* relaxation times, six pear fruits were longitudinally measured for about two months during the same period. The measurements for the harvested samples showed good agreement with the *in situ* measurements. From the measurements of the harvested samples, it is clear that the relaxation rates of the pear fruits linearly change with the inverse of the linear dimension of the fruits, demonstrating that the relaxation mechanism is a surface relaxation. We therefore conclude that the mobile MRI system is a useful device for measuring the NMR parameters of outdoor living plants.

1. Introduction

The major advantages of permanent magnets over superconducting magnets in nuclear magnetic resonance (NMR) and magnetic resonance imaging (MRI) are their portability, openness, and design flexibility, and that they do not require cryogenics. These advantages have opened up a wide variety of challenging and fascinating outdoor applications of NMR and MRI [1–11]. For example, NMR well-loggers and NMR MOUSE are typical successful outdoor NMR applications of permanent magnets. Another interesting recent topic is outdoor use of permanent-magnet MRI systems for plant studies.

Since the invention of MRI, most intact plant studies have been performed in laboratories or greenhouses [12–18]. These studies have yielded unique and valuable information about physiological states of the plants. However, MRI measurements of outdoor living plants have several advantages over indoor measurements. First, although it is difficult to control the ecological or physiological conditions for plants in outdoor or natural environments, their natural physiological status can be measured, which are very difficult to be achieved in laboratories or greenhouses. Second, the size of the plants measured using the MRI system need not be limited by the size of the laboratory or greenhouse. The third advantage is that no special or careful sample (plant) preparation for the laboratories, such as transportation or transplanting, is required.

However, there are several difficulties in the outdoor use of MRI systems for plant studies. First, it is not easy to set up delicate electronic instruments in outdoor environments because the weather and temperature often change suddenly, the environment is often dusty or muddy, and the ground is often rough and too soft to support heavy instruments such as permanent-magnet MRI machines. A second disadvantage is that it is usually difficult to position the plant samples precisely in the "sweet spot" of the MRI system because plants have various shapes, sizes, locations, and orientations, and are often fragile.

For these reasons, only a few studies have been reported for outdoor use of MRI systems for living plants. In 2006, Okada et al. reported outdoor MRI measurements of a living maple tree using a 0.3 T, 60 kg permanent magnet [19]. The results presented were promising but problems with external noise and the portability of the system remained unsolved. In 2011, Kimura et al. reported an electrically mobile MRI system with a flexible magnet-positioning system for the same 0.3 T magnet to image healthy and diseased branches of a Japanese pear tree in a research orchard [20]. They solved the above problems and succeeded in taking 24 h *in situ* measurements of apparent diffusion coefficient (ADC) images of the healthy branch. In 2012, Jones et al. reported an open access MRI system for living trees using a 0.026 T permanent

* Corresponding author. Fax: +81 29 853 5205.
E-mail address: kose@bk.tsukuba.ac.jp (K. Kose).

1090-7807/$ - see front matter © 2012 Elsevier Inc. All rights reserved.
http://dx.doi.org/10.1016/j.jmr.2012.10.012

magnet and succeeded in taking long-term outdoor MR measurements of a large tree (diameter ~90 mm) [21].

For outdoor MR measurements of fruit, in 2009, Kimura et al. reported *in situ* MRI measurements of Japanese pear fruit in a research orchard using a 0.12 T, 170 mm gap, and 160 kg permanent magnet [22]. They found that the image contrast of the T_1-weighted images of the pear fruit changed substantially over time during the growing stage (from June to August). However, although relaxation times are essential for acquiring high-quality MR images, no data were available on the relaxation times of the living pear fruit.

In this study, we developed an electrically mobile MRI system using a 0.2 T, 16 cm gap permanent magnet to acquire high-quality MR images than previously reported and performed longitudinal NMR parameter measurements of Japanese pear fruit during the cell enlargement period in a research orchard to assess the usefulness of the mobile MRI system.

2. Materials and methods

2.1. Mobile magnetic resonance imaging system

Fig. 1a shows the electrically mobile MRI system developed in this study. The core part of this system was constructed in the previous study [20] and the permanent magnet was replaced for this study. The mobile MRI system consists of a permanent magnet, a gradient coil set, a radiofrequency (RF) probe, an MRI console, a mobile lift, and an electrically motorised cart.

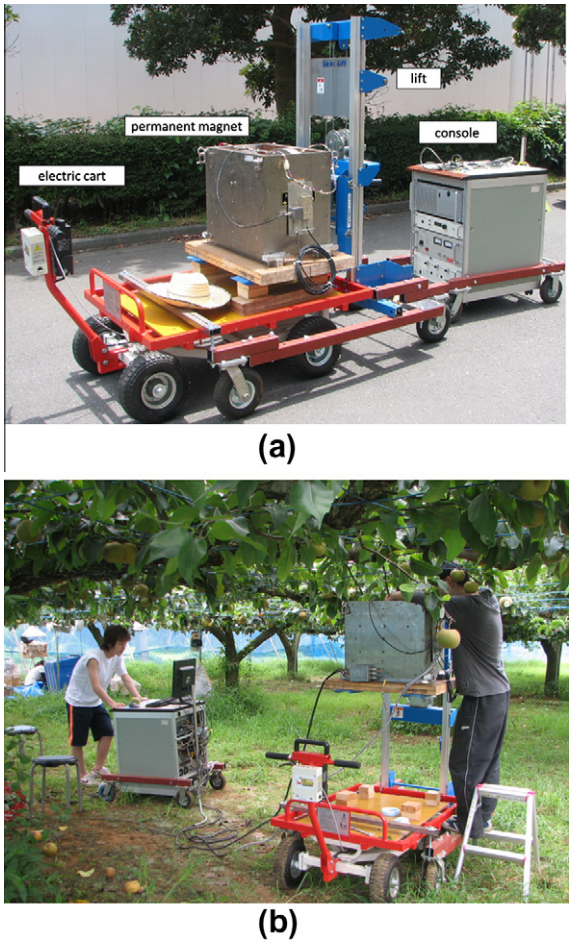

Fig. 1. (a) Overview of the electrically mobile MRI system developed in this study. The lift for the permanent magnet is mounted on the cart, which pulls the integrated MRI console. (b) *In situ* pear fruit measurements. The pear fruit is manually fixed in the RF coil.

The specifications of the permanent magnet (NEOMAX Engineering, Takasaki, Japan) are: magnetic field strength = 0.202 T; gap = 16 cm, homogeneity = 41.2 ppm over a 10 cm diameter spherical volume; size = 50.1 cm (width) × 36.0 cm (depth) × 44.0 cm (height); weight = 200 kg (Fig. 2). Because the magnet was originally developed for use in the International Space Station, it was designed to be as light as possible. The magnet was thermally insulated using several sheets of polyurethane foam about 5 mm thick to decrease the effect of rapid outdoor temperature changes. In addition, the inevitable Larmor frequency change caused by the temperature drift of the magnet was corrected using a time-sharing NMR lock technique.

We developed three planar gradient coil sets and six RF coils for various sizes of growing pear fruit. The specifications of the gradient coils are tabulated in Table 1. All of the transverse (Gx and Gy) gradient coils and the largest axial (Gz) gradient coil were designed using the target field method [23] and the axial gradient coils for the number 1 and 2 coil sets were designed using a genetic algorithm to maximise the homogeneous region. The number 1 and 2 gradient coil sets were fixed within the gap of the magnet and the number 3 coil set was attached to the pole pieces of the magnet, as shown in Fig. 2. The maximum gradient strength for Gx, Gy, and Gz coils were 64, 64, and 150 mT/m for the coil number 1, 54, 52, and 80 mT/m for the coil number 2, and 13.6, 13.6, and 31 mT/m for the coil number 3. The RF coils were solenoids having diameters of 26, 32, 38, 54, 90, and 108 mm. The MRI console (total weight about 100 kg) was developed in our laboratory and its control software was developed by MRTechnology Inc. (Tsukuba, Japan).

The electric cart (CB-02, Yamaichi-Seikou Co. Ltd., Suzaka, Japan) driven by a Ni–H battery and the mobile lift (GL-4, Genie Industries, WA, USA) were combined to carry and lift the magnet as shown in Fig. 1a. The maximum height and bearing weight of

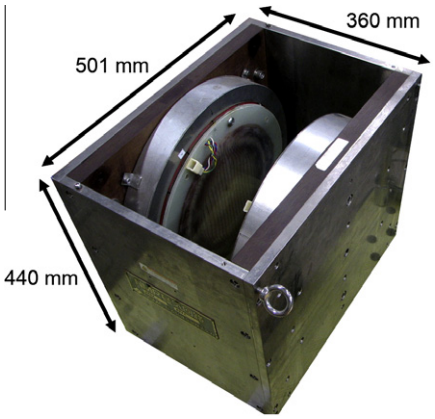

Fig. 2. The 0.2 T permanent magnet used in this study. The yoke was made of 15.5 mm thick iron plates to reduce the weight of the magnet and reinforced with 29.5 mm thick Bakelite plates. A three-channel planar gradient coil set was attached to the pole pieces of the magnet.

Table 1
Specifications of the gradient coils developed in this study.

Coil no.	Gap (mm)	Gx efficiency	Gy efficiency	Gz efficiency
1	50	6.4	6.4	15.0
2	76	5.4	5.2	8.0
3	150	1.36	1.36	3.1

Efficiency: mT m^{-1} A^{-1}.

the fork of the lift were 140 cm and 225 kg, respectively. The running distance of the cart per charge was about 6 km.

2.2. Pear fruit

All of the pear fruit used in this study were from a Japanese pear tree (*Pyrus pyrifolia* Nakai, Kosui), about 35 year-old, grown in a research orchard in the Agricultural and Forestry Research Centre of the University of Tsukuba, located about 1.5 km from our laboratory. This pear tree bears several hundred fruits every year.

To measure the relaxation times and ADC of the pear fruit in relation to their weight, seven pear fruits were harvested and measured in the research orchard almost every week. We started the measurements on May 25 and finished on August 23. The seven pear fruits included the lightest and heaviest fruit that could be found on the day of the measurements, and five with weights distributed as evenly as possible between those of the lightest and the heaviest.

For *in situ* measurements, we used six pear fruits that were growing near the ends of branches of the pear tree and had relatively long stalks, as these factors made them suitable for *in situ* NMR measurements. These fruits were close to the average size when we started the measurements. They were manually fixed near the centre of the RF probe, as shown in Fig. 1b. We started these measurements on June 25 and finished on August 19.

3. Experiments

3.1. Relaxation time measurements

The T_1 of the pear fruit was measured using the inversion recovery (IR) sequence. The TR (repetition time) of the IR sequence was varied from 4000 to 11,000 ms to exceed the estimated T_1 values by about six times and the spin echo signal with TE (echo time) = 12 ms was measured. Because the IR signal was found to fit a single IR curve very well in the preliminary experiments, we used the null method to measure T_1 in the orchard to save measurement time.

The T_2 of the pear fruit was measured using the Carr–Purcell–Meiboom–Gill (CPMG) sequence. Table 2 shows the parameters used for the CPMG measurements. These parameters were determined by the following factors: the homogeneity of the magnet (41.2 ppm over 10 cm diameter spherical volume), corresponding to about 350 Hz spectral width for homogeneous and spherical specimens, spectral width due to the susceptibility distribution of the pear fruit (at most 10 ppm or 100 Hz), RF pulse width (120 μs) for 90° and 180° pulses, which are reasonable width for the 10.8 cm diameter RF coil and the 100 W RF transmitter. Because the signal to noise ratio of the CPMG signal was sufficient for relaxation time measurements, no signal averaging was performed. The spin echo peak signal was fitted using two exponentially decaying signals with different amplitudes and T_2 values.

As the MRI system was not waterproof, we performed the experiments only on sunny days and cloudy days, although there were many rainy days during the research period.

3.2. ADC measurements

ADC values were measured using the Stejskal–Tanner pulsed gradient spin-echo sequence [24] with 64 or 128 steps with equal increments of the field gradient parallel to the fruit axis. For smaller samples (diameter < 40 mm), δ (the length of two equal pulsed field gradients), Δ (the time between the pulsed field gradients applied before and after the 180° RF pulse), TE, and TR were 25, 30, 60, and 800 ms, respectively. The largest b value ($=\gamma^2 G^2 \delta^2 (\Delta - \delta/3)$) was about 990 smm^{-2}. For larger samples (diameter > 40 mm), δ, Δ, TE, and TR were 28, 32, 64, and 1200 ms, respectively. The largest b value was about 860 smm^{-2}. The spin echo amplitude was found to fit a single exponential decay curve with the b value very well. For several pear fruits, ADC values were measured with various Δ (20–200 ms).

Because the ADC values were sensitive to the temperature of the fruit, dependent on the air temperature in the orchard, and relatively insensitive to the time after harvest, we used ADC values measured in the laboratory (room temperature ~26 °C) on the day of the harvest for the quantitative analysis.

4. Results

4.1. System performance

We measured the pear fruit in the research orchard and our laboratory almost every week using our MRI system, because it was very easy to shuttle the MRI system between the two places. It took about 20 min for us to drag the mobile MRI system from the laboratory to the orchard. It was also easy to move the MRI system within the orchard, even though the ground was rough and soft for the heavy permanent-magnet system (~300 kg including the lift and the cart). The integrated compact MRI console was also useful for quick setup of the MRI system, because the cable connection time was minimised (several minutes).

The NMR frequency drift in the orchard was less than a few kHz/h, corresponding to a few one-tenth degrees per hour temperature-change of the magnet. Because the measurement time for the relaxation time (T_1 or T_2) was less than a few minutes, no RF coil re-tuning was required in the orchard.

4.2. Imaging experiments

Fig. 3 shows a two-dimensional cross-section selected from a three-dimensional (3D) image dataset of a pear fruit harvested on August 23 acquired with a 3D spin-echo sequence (field of

Table 2
Parameters for T_2 measurements.

Date	TR (ms)	TE (ms)	No. of echoes	Dwell time (μs)	No. of samples	Samples per echo
5/25	1000	20	14	600	512	33
6/01	3000	20	20	400	1024	50
6/08	3000	20	20	400	1024	50
6/15	3000	20	20	400	1024	50
6/22	3000	20	20	400	1024	50
6/29	3000	20	20	400	1024	50
7/06	3000	40	14	600	1024	66
7/13	3000	40	14	600	1024	66
7/22	3000	40	20	400	2048	100
8/01	3000	40	20	400	2048	100
8/10	4500	60	20	600	2048	100
8/23	4500	60	20	600	2048	100

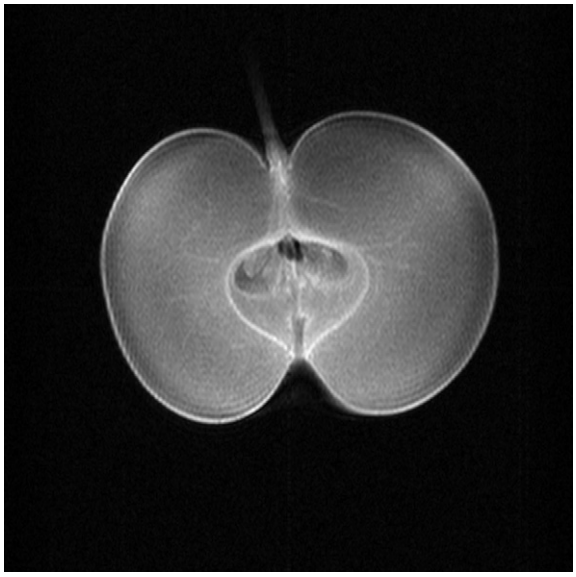

Fig. 3. A 2D cross-section selected from a 3D image dataset of a pear fruit acquired with a 3D spin echo sequence. Field of view = 128 × 128 × 128 mm, image matrix = 256 × 256 × 16, repetition time = 400 ms, spin echo time = 20 ms, number of signals averaged = 4, total measurement time = 1.8 h.

view = 128 × 128 × 128 mm, image matrix = 256 × 256 × 16, repetition time = 400 ms, spin echo time = 20 ms, number of signals averaged = 4, total measurement time = 1.8 h). This image clearly demonstrates the capability of this system to generate high-quality images of excised pear fruit in the laboratory.

4.3. NMR parameter measurements and pear fruit weight

Fig. 4 shows the weights of the pear fruits used for the NMR parameter measurements related to their measurement dates. This figure clearly shows that both the average and distribution of the weights increase rapidly with time.

Fig. 5 shows spin echo data acquired by the CPMG sequences for the smallest (diameter = 2 cm) and the largest (diameter = 10 cm) pear fruit measured on May 25 and August 23. The shape of the spin echo signal seems mostly determined by the inhomogeneity of the magnet, because the bulk T_2^* of the largest pear fruit was about 4 ms, corresponding to about 100 Hz half spectral width, consistent with about 350 Hz total spectral width caused by the magnet inhomogeneity. The apparently exponentially decaying curve observed in Fig. 5, which was actually divided into two decaying components, suggests that the decay of the spin echo

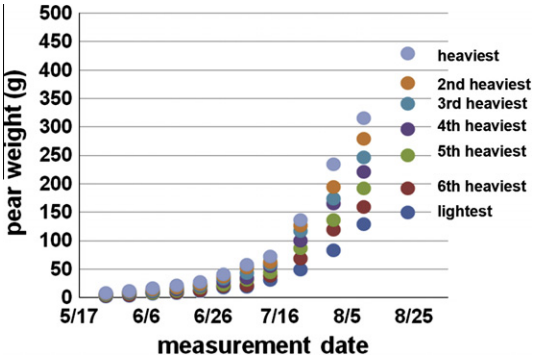

Fig. 4. Weights of the harvested pear fruit used for the longitudinal NMR measurements.

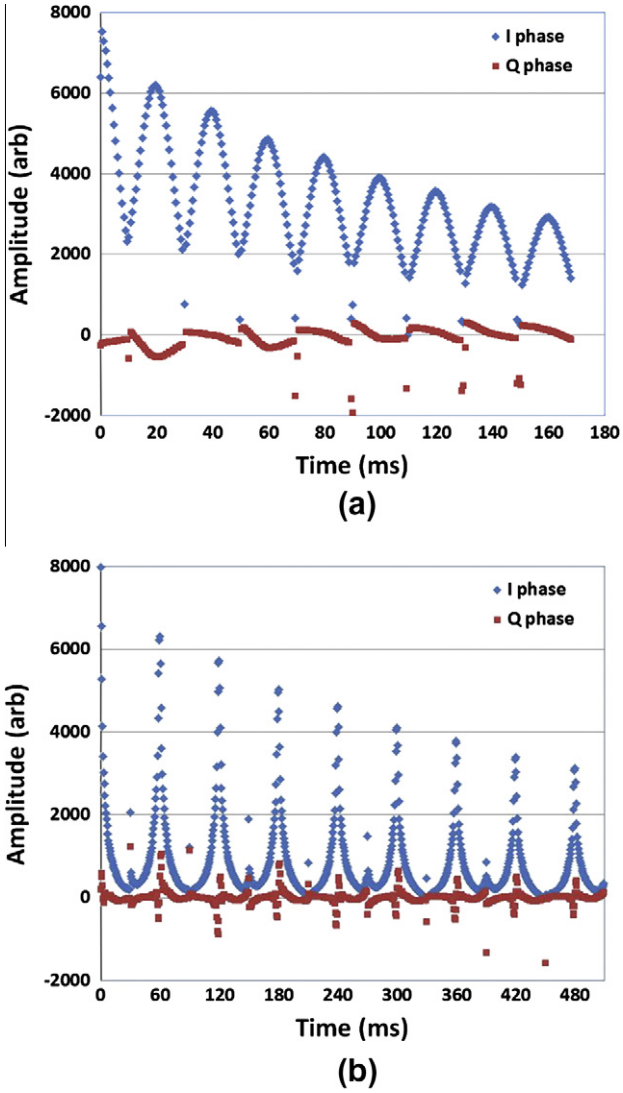

Fig. 5. Spin echo data acquired by the CPMG sequences. (a) The smallest (diameter ~ 2 cm) pear fruit measured on May 25. (b) The largest (diameter ~ 10 cm) pear fruit measured on August 23.

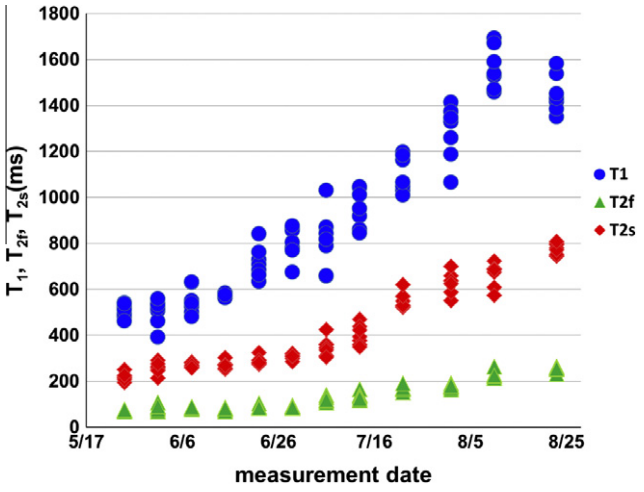

Fig. 6. T_1 (blue), T_{2f} (green), and T_{2s} (red) of the pear fruit measured just after harvest plotted against the harvest date. (For interpretation of the references to colour in this figure legend, the reader is referred to the web version of this article.)

signal was not affected by the diffusion of the water molecules in the pear fruit, because the local magnetic field gradients are small in the low (0.2 T) magnetic field.

Fig. 6 shows the single T_1 value and two T_2 values, T_{2f} and T_{2s} for fast and slow T_2 relaxation components, measured for the pear fruit plotted against the harvest (measurement) date, showing a rapid increase with time similar to the weights shown in Fig. 4.

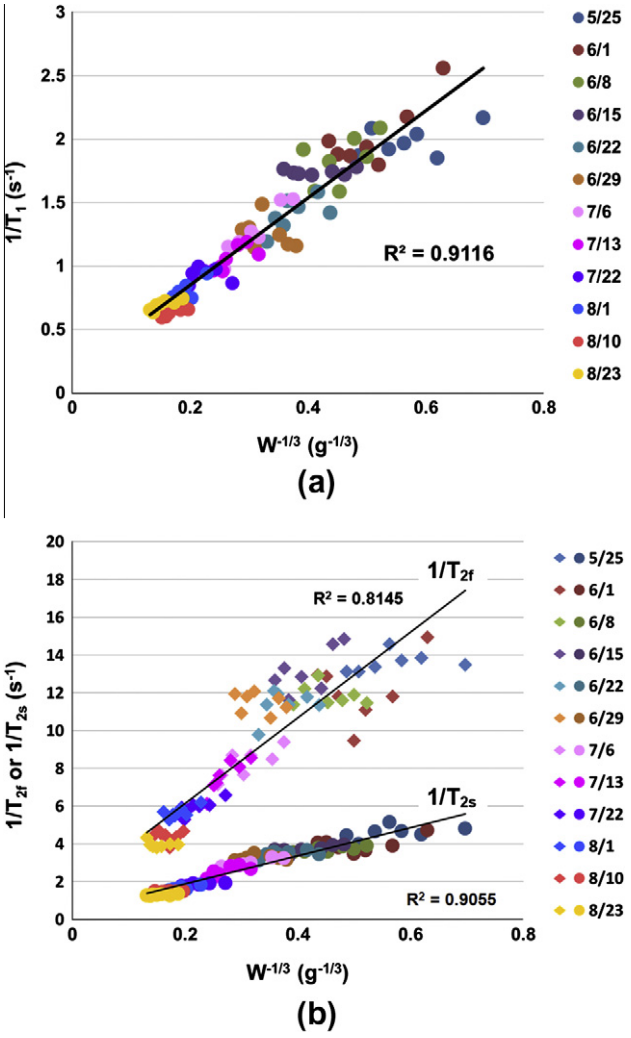

Fig. 7. $1/T_1$ (a), and $1/T_{2f}$ and $1/T_{2s}$ (b) plotted against the inverse of the cube root of the pear fruit weight.

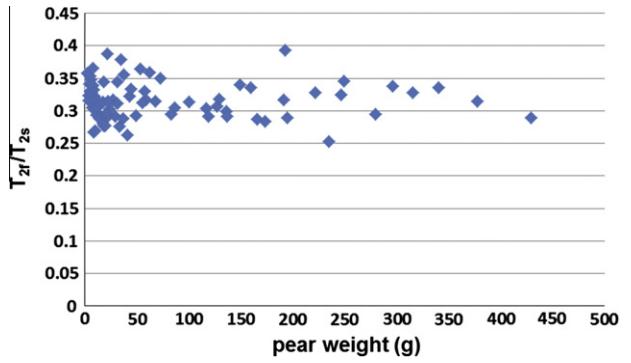

Fig. 8. Signal strength for the protons with the faster T_2 relaxation time normalised by that for slower T_2 plotted against the harvest date.

Fig. 7 shows the relaxation rates plotted against the inverse of the cube root of the weight, showing good linear relations, especially for T_1 and T_{2s}. Fig. 8 shows the signal strength for the protons with the faster T_2 relaxation time normalised by that for the slower T_2 plotted against the harvest date. This graph clearly shows that the proportion of the protons with different T_2 values was nearly constant.

Fig. 9 shows the ADC values plotted against Δ for a pear fruit harvested on June 8. This graph clearly shows the restricted

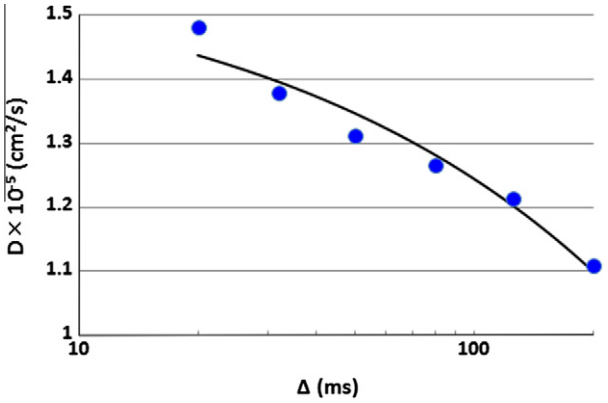

Fig. 9. ADC plotted against Δ measured for a small pear fruit.

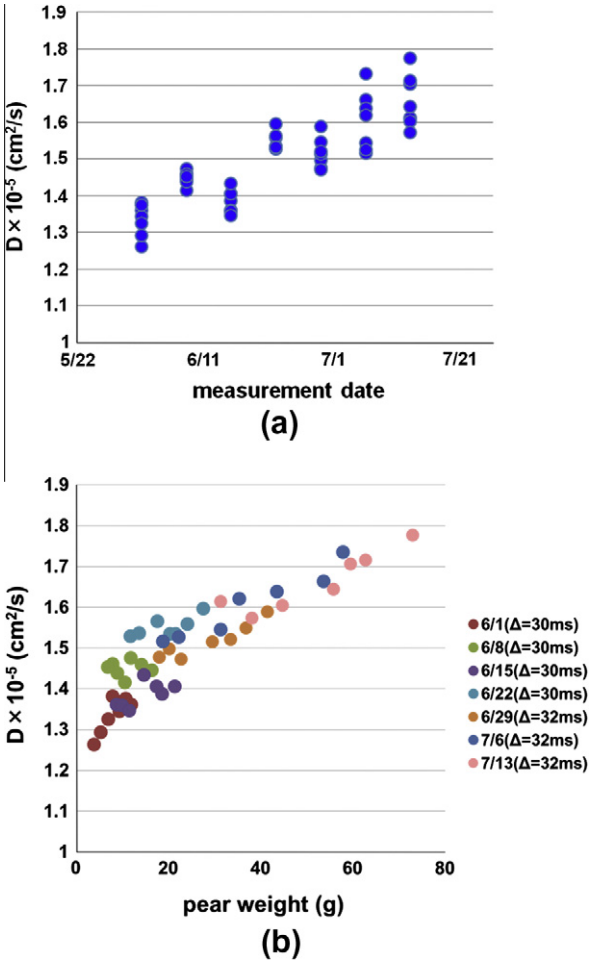

Fig. 10. ADC at Δ = 30 or 32 ms plotted against the harvest date (a), and against pear fruit weight (b).

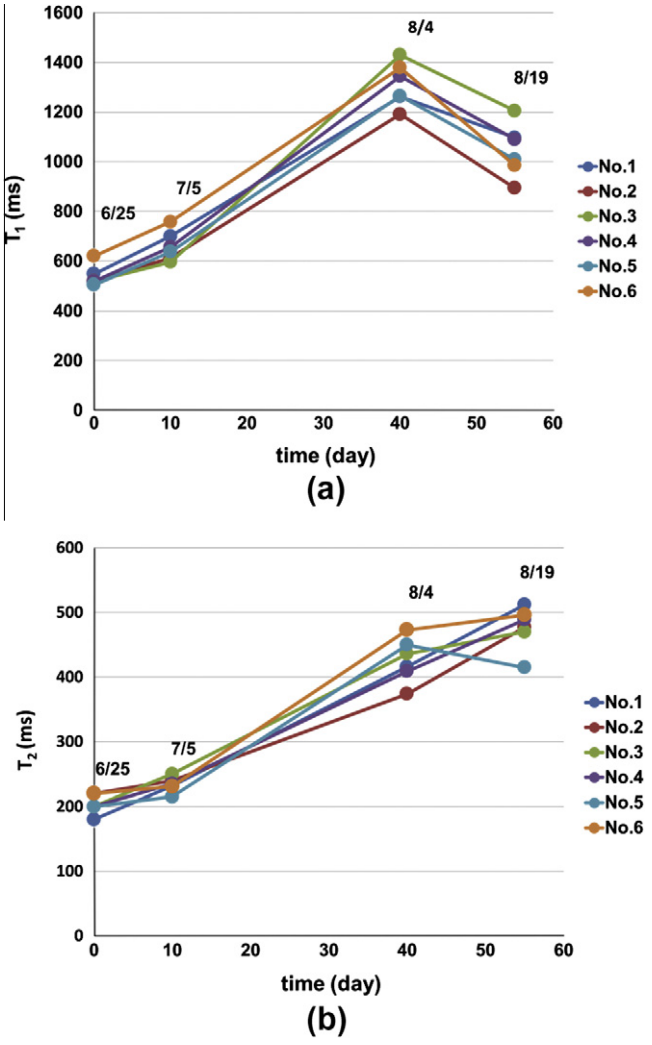

Fig. 11. T_1 (a) and T_2 (b) of six pear fruits measured *in situ* during the growing process.

diffusion effect. Fig. 10a and b shows the ADC values measured for $\Delta = 30$ or 32 ms plotted against the measurement date and the weight. Fig. 10b clearly demonstrates that the ADC increases with the weight of the fruit.

4.4. In situ measurements

Fig. 11 shows the T_1 and T_2 of six pear fruits measured *in situ*. The T_2 values are plotted only for the slower T_2 relaxation component. As these graphs show, the relaxation times initially increase rapidly with time, similar to those observed for the harvested pear fruits. However, a slight decrease in the T_1 on August 19 is evident. A similar decrease is also seen for the harvested samples, as shown in Fig. 6.

5. Discussion

5.1. NMR parameters measured in relation to the pear fruit weight

The growth stage of the Japanese pear fruit is divided into a cell division period and a cell enlargement period [25]. The cell division period runs from early May and terminates to late May. The cell enlargement period runs from late May to late August. Therefore, our NMR experiments were performed during the cell enlargement period.

The enlargement of the fruit cells is accompanied by that of the vacuole of the fruit cell, and the slow component of the T_2 relaxation times shown in Fig. 7b are considered to be those of the water protons in the vacuole [26,27]. Fig. 7 clearly shows that the quantity $1/T_{2s}$ has a linear relationship with the inverse of the size of the vacuole (~cube root of the weight). Therefore, we think that Fig. 7b shows that the transverse relaxation of the water protons in the vacuole of the pear fruit is mostly determined by the surface relaxation on the boundary of the vacuole [28,29]. A similar relationship was reported for the cells in the apex zone of the stems of intact maize and pearl millet plants in 2001 [30].

As shown in Fig. 10, the ADC at $\Delta = 30$ or 32 ms increases monotonically with the pear weight. We think this increase is caused by the fact that the restricted diffusion became less effective as the cell size increased. If we had been able to measure the ADC for a much wider range of Δ for all pear samples, we could have obtained information about the size of the vacuole and the water membrane permeability, as described in earlier reports [17,31]. However, we could not perform these measurements, mainly because of the limitations of the hardware and measurement time.

5.2. In situ measurements

There have been many studies of relaxation time measurements of fruits in different growth stages [32,33], in which it was also reported that the relaxation times lengthen with the growing term of the fruit. As far as we know, this study is the first to report relaxation times of identical growing fruits measured *in situ* during the growth stage.

However, compared with the relaxation time measurements of the harvested pear fruit, the accuracy of the *in situ* relaxation time measurements may be limited because the fruits were manually fixed in the RF probe. Therefore, if we manage to develop a good fixing device, the accuracy of the measurements would be further improved and *in situ* MRI would be possible for 3D measurements of the fruit size. The development of such a fixing device will be the subject of future research.

As shown in Figs. 4 and 9, a slight decrease in the T_1 was observed. This decrease may be due to an increase in viscosity caused by the increase in sugar in the vacuole. However, a further study will be required to clarify this phenomenon.

6. Conclusions

We measured the relaxation times and ADC of protons of Japanese pear fruits using an electrically mobile MRI system during the cell enlargement period. The relaxation times were measured both *in situ* and for harvested pear fruits in relation to their weight. The temporal changes in the relaxation times for the harvested pear fruits showed good agreement with those for the *in situ* measurements. We observed that the relaxation rates had good linear relations with the inverse of the cube root of the pear fruit weight, demonstrating that the relaxation mechanism is the surface relaxation. We therefore conclude that the mobile MRI system is a useful device for measurements of outdoor living plants.

References

[1] R.K. Cooper, J.A. Jackson, Remote (inside-out) NMR. I. Remote production of a region of homogeneous magnetic field, J. Magn. Reson. 41 (1980) 400–405.
[2] L.J. Burnett, J.A. Jackson, Remote (inside-out) NMR. II. Sensitivity of NMR detection for external samples, J. Magn. Reson. 41 (1980) 406–410.
[3] J.A. Jackson, L.J. Burnett, F. Harmon, Remote (inside-out) NMR. III. Detection of nuclear magnetic resonance in a remotely produced region of homogeneous magnetic field, J. Magn. Reson. 41 (1980) 411–421.
[4] R.F. Paetzold, G.A. Matzkanin, A. De Los Santos, Surface soil water content measurement using pulsed nuclear magnetic resonance techniques, Soil Sci. Soc. Am. J. 49 (1985) 537–540.

[5] H. Van As, J.E.A. Reinders, P.A. de Jager, P.A.C.M. van de Sanden, T.J. Schaafsma, *In situ* plant water balance studies using a portable NMR spectrometer, J. Exp. Bot. 45 (1994) 61–67.
[6] G. Eidmann, R. Savelsberg, P. Blümler, B. Blümich, The NMR MOUSE, a mobile universal surface explorer, J. Magn. Reson. A122 (1996) 104–109.
[7] E. Fukushima, J.A. Jackson, Unilateral magnet having a remote uniform field region for nuclear magnetic resonance, US Patent 6,489,872, 2002.
[8] B. Manz, A. Coy, R. Dykstra, C.D. Eccles, M.W. Hunter, B.J. Parkinson, P.T. Callaghan, A mobile one-sided NMR sensor with a homogeneous magnetic field: the NMR-MOLE, J. Magn. Reson. 183 (2006) 25–31.
[9] A.E. Marble, I.V. Mastikhin, B.G. Colpitts, B.J. Balcom, A compact permanent magnet array with a remote homogeneous field, J. Magn. Reson. 186 (2007) 100–104.
[10] J. Perlo, F. Casanova, B. Blümich, Ex situ NMR in highly homogeneous fields: H-1 spectroscopy, Science 315 (2007) 1110–1112.
[11] B. Blümich, J. Perlo, F. Casanova, Mobile single-sided NMR, Prog. Nucl. Magn. Reson Spectrosc. 52 (2008) 197–269.
[12] H. Van As, T.J. Schaafsma, Noninvasive measurement of plant water-flow by nuclear magnetic resonance, Biophys. J. 45 (1984) 469–472.
[13] N. Ishida, M. Koizumi, H. Kano, The NMR microscope, a unique and promising tool for plant science, Ann. Bot. 86 (2000) 259–278.
[14] M. Rokitta, E. Rommel, U. Zimmermann, A. Haase, Portable nuclear magnetic resonance imaging system, Rev. Sci. Instrum. 71 (2000) 4257–4262.
[15] W. Köckenberger, Functional imaging of plants by magnetic resonance experiments, Trends Plant Sci. 6 (2001) 286–292.
[16] S. Utsuzawa, K. Fukuda, D. Sakaue, Use of magnetic resonance microscopy for the non-destructive observation of xylem cavitation caused by pine wilt disease, Phytopathology 95 (2005) 737–743.
[17] H. Van As, Intact plant MRI for the study of cell water relations, membrane permeability, cell-to-cell and long-distance water transport, J. Exp. Bot. 58 (2007) 743–756.
[18] C.W. Windt, H. Soltner, D. van Dusschoten, P. Bluemler, A portable Halbach magnet that can be opened and closed without force. The NMR-CUFF, J. Magn. Reson. 208 (2011) 27–33.
[19] F. Okada, S. Handa, S. Tomiha, K. Ohya, K. Kose, T. Haishi, S. Utsuzawa, K. Togashi, Development of a portable MRI for outdoor measurements of plants, in: The 6th Colloquium on Mobile Magnetic Resonance, Aachen, Germany, 6–8 September, 2006.
[20] T. Kimura, Y. Geya, Y. Terada, K. Kose, T. Haishi, H. Gemma, Y. Sekozawa, Development of a mobile magnetic resonance imaging system for outdoor tree measurements, Rev. Sci. Instrum. 82 (2011) 053704.
[21] M. Jones, P.S. Aptaker, J. Cox, B.A. Gardiner, P.J. McDonald, A transportable magnetic resonance imaging system for *in situ* measurements of living trees: the Tree Hugger, J. Magn. Reson. 218 (2012) 133–140.
[22] T. Kimura, D. Tamada, S. Handa, K. Kose, T. Haishi, K. Togashi, H. Gemma, Y. Sekozawa, Development of a portable MRI system for fruits and trees, in: The 10th International Conference on Magnetic Resonance Microscopy, West Yellowstone, USA, 30 August–4 September, 2009.
[23] R. Turner, A target field approach to optimal coil design, J. Phys. D: Appl. Phys. 19 (1986) L147–L151.
[24] E.O. Stejskal, J.E. Tanner, Spin diffusion measurements: spin echoes in the presence of a time-dependent field gradient, J. Chem. Phys. 42 (1965) 288–292.
[25] M.N. Westwood, Temperate-Zone Pomology, W. H. Freeman and Co. San Francisco, USA, 1978.
[26] B.P. Hills, S.L. Duce, The influence of chemical and diffusive exchange on water proton transverse relaxation in plant tissues, Magn. Reson. Imag. 8 (1990) 321–331.
[27] J.E.M. Snaar, H. Van As, Probing water compartments and membrane permeability in plant cells by ^{1}H NMR relaxation measurements, Biophys. J. 63 (1992) 1654–1658.
[28] K.R. Brownstein, C.E. Tarr, Importance of classical diffusion in NMR studies of water in biological cells, Phys. Rev. A19 (1979) 2446–2453.
[29] L. van der Weerd, S.M. Melnikov, F.J. Vergeldt, E.G. Novikov, H. Van As, Modelling of self-diffusion and relaxation time NMR in multi-compartment systems with cylindrical geometry, J. Magn. Reson. 156 (2002) 213–221.
[30] L. van der Weerd, M.M.A.E. Claessens, T. Ruttink, F.J. Vergeldt, T.J. Schaafsma, H. Van As, Quantitative NMR microscopy of osmotic stress responses in maize and pearl millet, J. Exp. Bot. 52 (2001) 2333–2343.
[31] P.N. Sen, Time-dependent diffusion coefficient as a probe of geometry, Concept. Magnetic Res. 23A (2004) 1–21.
[32] C.J. Clark, L.N. Drummond, J.S. MacFall, Quantitative NMR imaging of kiwifruit (*Actinidia deliciosa*) during growth and ripening, J. Sci. Food. Agric. 78 (1998) 349–358.
[33] C.J. Clark, J.S. MacFall, Quantitative magnetic resonance imaging of 'Fuyu' persimmon fruit during development and ripening, Magn. Reson. Imag. 21 (2003) 679–685.